URSI-B EMTS 2025, Bologna, 23–27 June

Frequency-selective Dynamic Scattering Arrays for Over-the-air EM Processing

D. Dardari[(1)]
(1) DEI, University of Bologna and WiLab-CNIT, Cesena Campus, Cesena (FC), Italy - e-mail: davide.dardari@unibo.it

Abstract

In this paper, we investigate frequency-selective dynamic scattering array (DSA), a versatile antenna structure capable of performing joint wave-based computing and radiation by transitioning signal processing tasks from the digital domain to the electromagnetic (EM) domain. The numerical results demonstrate the potential of DSAs to produce space-frequency superdirective responses with minimal usage of radiofrequency (RF) chains, making it particularly attractive for future holographic multiple-input multiple-output (MIMO) systems.

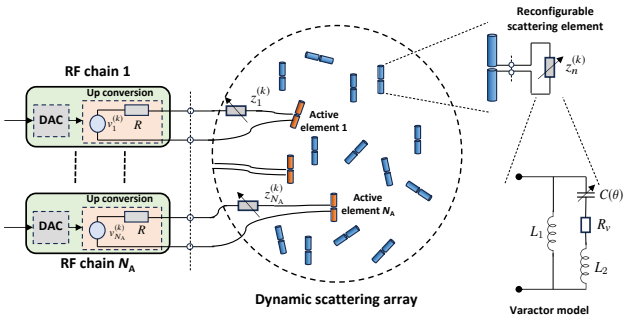

Figure 1. Schematic of the DSA.

1 Introduction

The use of high-frequency bands in the millimeter wave and THz ranges, combined with the integration of antennas with a large number of elements, is driving current wireless technology toward seemingly insurmountable challenges in hardware complexity, latency, and power consumption. These issues present significant obstacles to the sustainability of future wireless networks.

One promising strategy for enhancing sustainability is to shift part of the signal processing directly to the electromagnetic (EM) domain, a concept known as electromagnetic signal and information theory (ESIT) [1–3]. This can be achieved by designing reconfigurable EM environments [4] using advanced EM metamaterial devices to perform basic processing functions [5], reconfigurable intelligent surfaces (RISs), or the recently introduced stacked intelligent metasurfaces (SIMs) [6]. In particular, the study of SIMs remains in its early stages, and the key technological and modeling challenges are yet to be fully addressed. For example, the spacing between layers must span several wavelengths to ensure the validity of the cascade model currently in use. Additionally, power losses and signal distortion caused by the multiple layers and the bounding box require further investigation. A notable limitation of SIMs is that only the final layer radiates, restricting the characteristics of the generated EM waves to those achievable with a conventional planar surface or array. Meanwhile, the hidden layers are primarily responsible for performing EM transformations.

To address the aforementioned limitations, we investigate an EM antenna structure, referred to as a dynamic scattering array (DSA), which offers significant flexibility by enabling advanced processing capabilities directly at the EM level while radiating [7]. A DSA comprises a limited number of active antenna elements, each connected to an RF chain (input), and is surrounded by a cluster of many reconfigurable passive scatterers. These scatterers interact within the reactive near field, enabling EM processing and radiation to occur jointly "over the air". A DSA can be viewed as a generalization of reactively controlled arrays, initially introduced in [8], and their evolution into electrically steerable passive array radiators (ESPARs), which utilize a single RF chain [9].

In this paper, we extend the concept of DSA to operate with wideband signals, thereby enabling space-frequency processing capabilities. Additionally, unlike previous works on DSA, we eliminate the requirement for ideal loads and a perfectly reconfigurable matching network by introducing reconfigurable loads modeled as a realistic varactor diode. Building on the analytical expression of the frequency-dependent characteristics of the DSA as a function of its configuration parameters, we formulate an optimization problem to design these parameters according to the desired space-frequency response. Numerical results highlight the remarkable flexibility of the DSA in realizing different beams each associated with a different port and frequency while offering significant advantages with respect to current holographic MIMO solutions, such as reduced size and minimized number of RF chains. For example, we demonstrate that the tight coupling of DSA elements enables the realization of superdirectivity, regardless of the beam's direction - a capability that stands in contrast to standard arrays, where superdirectivity is typically limited to the end-fire direction.

2 Frequency-selective Dynamic Scattering Array Modelling

With reference to Fig. 1, a DSA is composed of N antenna elements of which N_A are active and hence connected to an RF chain, and $N_\mathrm{S} = N - N_\mathrm{A}$ are passive scattering antenna elements [7]. We consider a multicarrier system with total bandwidth W using K subcarriers at frequencies $f_k = f_0 + (k-1)W/K$, for $k = 1,2,\dots K$. At the generic kth sucarrier, the N_A RF chains introduce open circuit voltages $\mathbf{v}^{(k)} = \left[v_1^{(k)}, v_2^{(k)}, \dots, v_{N_\mathrm{A}}^{(k)}, 0, 0, \dots, 0\right]^\mathrm{T}$ to the first N_A elements that carry the information. The response of the DSA can be changed by loading each antenna element with reconfigurable loads of impedances $z_n^{(k)}(\theta_n)$, with $n = 1,2,\dots N$, where θ_n is a parameter to be optimized, as it will be detailed later. Denote with $\boldsymbol{\theta} = \{\theta_n\}_{n=1}^N$ the set of optimization parameters. Ideally, the loads should be designed to be only reactive to avoid power losses. At the kth subcarrier, the overall DSA system can be modeled as an N-port network in which the following relationship between the set of currents $\mathbf{i}^{(k)}$ and open circuit voltages $\mathbf{v}^{(k)}$ is given by

$$\left(\mathbf{Z}_\mathrm{L}^{(k)}(\boldsymbol{\theta}) + \mathbf{Z}^{(k)}\right)\mathbf{i}^{(k)} = \mathbf{v}^{(k)} \tag{1}$$

where $\mathbf{Z}^{(k)} \in \mathbb{C}^{N\times N}$ is the impedance matrix of the antenna structure and $\mathbf{Z}_\mathrm{L}^{(k)}(\boldsymbol{\theta}) = \{z_n^{(k)}(\theta_n)\}_{n=1}^N$ represents the set of reconfigurable loads' impedances. All the interactions between the elements of the DSA are captured by the impedance matrix $\mathbf{Z}^{(k)}$, which does not depend on the reconfigurable loads, and relates the voltages and currents of the N ports. For instance, with Hertzian dipoles or half-wave dipoles, it can be computed analytically [10].

Consider now T test points located in positions $\mathbf{p}_t$, with $t = 1,2,\dots,T$, and that in each test point, a conventional receiving antenna is used to probe the signal with gain $\mathbf{G}_\mathrm{R}$. As commonly done in the literature, we assume that the test points are located in the radiative region of the DSA and the receiving antennas do not affect the transmitting DSA. As an example, the set of T antennas might represent a conventional receiving antenna array of a MIMO system. The end-to-end relationship between the open circuit voltages at the N_A ports and the useful component (i.e., without noise) of the received signal $\mathbf{y}^{(k)} = \left[y_1^{(k)}, y_2^{(k)}, \dots, y_T^{(k)}\right]^\mathrm{T}$ at the test positions for subcarrier k is

$$\mathbf{y}^{(k)} = \mathbf{H}_c^{(k)}\mathbf{i}^{(k)} = \mathbf{H}_c^{(k)}\left(\mathbf{Z}_\mathrm{L}^{(k)}(\boldsymbol{\theta}) + \mathbf{Z}^{(k)}\right)^{-1}\mathbf{v}^{(k)} \tag{2}$$

where $\mathbf{H}_c^{(k)} \in \mathbb{C}^{T\times N}$ is the transimpedance matrix of the radio channel accounting for the propagation effects that can be easily computed analytically in free-space conditions. The previous equation can be used as a general model for the DSA in an optimization problem to determine the set of parameters $\boldsymbol{\theta}$ once the desired response $\mathbf{y}^{(k)}$ is fixed for each subcarrier.

Define the matrix $\mathbf{V} = \sqrt{4R}\,\mathrm{diag}(1,2,\dots,N_\mathrm{A}) \in \mathbb{R}^{N\times N_\mathrm{A}}$, being R the internal resistance of the RF chains. Indicating with $\mathbf{i}_n^{(k)} = \left(\mathbf{Z}_\mathrm{L}^{(k)}(\boldsymbol{\theta}) + \mathbf{Z}^{(k)}\right)^{-1}[\mathbf{V}]_{(:,n)}$ the current in the case only the nth RF chain is excited at subcarrier k, where $[\mathbf{V}]_{(:,n)}$ represents the nth column of $\mathbf{V}$, the corresponding radiated power results $P_{\mathrm{rad},n}^{(k)} = \left(\mathbf{i}_n^{(k)}\right)^\mathrm{H}\Re\{\mathbf{Z}\}\,\mathbf{i}_n^{(k)}$, with $\Re\{x\}$ being the real part of x and $(\cdot)^\mathrm{H}$ the conjugate transpose operator. The factor $\sqrt{4R}$ in matrix $\mathbf{V}$ has been introduced to normalize the power available at each RF chain and subcarrier to 1 W. Because of the losses and possible impedance mismatch between the RF chains and the DSA at the N_A input ports, the efficiency of the DSA is, in general, less than one, then $P_{\mathrm{rad},n}^{(k)} \le 1\,\mathrm{W}$.

In general, one may aim to solve the following optimization problem for given objective end-to-end channel matrices $\mathbf{H}_{\mathrm{opt}}{}^{(k)} \in \mathbb{C}^{T\times N_\mathrm{A}}$, $k = 1,2,\dots,K$,

$$\hat{\boldsymbol{\theta}} = \arg\min_{\boldsymbol{\theta}} \sum_{k=1}^{K} \left\| \alpha^{(k)}\,\mathbf{H}_c^{(k)}\left(\mathbf{Z}_\mathrm{L}^{(k)}(\boldsymbol{\theta}) + \mathbf{Z}^{(k)}\right)^{-1}\mathbf{V} - \mathbf{H}_{\mathrm{opt}}{}^{(k)} \right\|_\mathrm{F}^2 \tag{3}$$

where $\alpha^{(k)}$ is a normalization constant, and $\|\cdot\|_\mathrm{F}$ denotes the Fronebous norm. The tth row of $\mathbf{H}_{\mathrm{opt}}{}^{(k)}$ represents the desired end-to-end channel response associated with the nth port and the kth subcarrier of the DSA. It is worth noticing that with the same configuration $\hat{\boldsymbol{\theta}}$ of the DSA, $N_\mathrm{A}\times K$ different space-frequency responses are obtained simultaneously, each one associated with one specific subcarrier and the input port of one specific RF chain.

Regarding the reconfigurable load, we consider a varactor diode whose circuit model is reported in Fig. 1 (right-bottom) as suggested in [11]. The corresponding impedance is

$$z_n^{(k)}(\theta_n) = \frac{j2\pi f_k L_1\left(j2\pi f_k L_2 + 1/(j2\pi f_k C(\theta_n)) + R_v\right)}{j2\pi f_k (L_1+L_2) + 1/(j2\pi f_k C(\theta_n)) + R_v} \tag{4}$$

where $C(\theta) = C_\mathrm{min} + (C_\mathrm{max} - C_\mathrm{min})(\tan^{-1}(\theta) + \pi/2)/\pi$, being C_min and C_max, respectively, the minimum and maximum capacitance of the varactor. The relationship between the optimization parameter θ and C has been chosen so that θ is unbounded and the optimization problem in (3) becomes unconstrained, thus making its numerical solution computation faster. For convenience, we embed in $z_n^{(k)}(\theta_n)$, for $n = 1,2,\dots N_\mathrm{A}$, also the internal resistance R of the RF chain. In the numerical results, the following parameters have been considered: $R_v = 0.1\,\Omega$, $L_1 = 2.5\,\mathrm{nH}$, $L_2 = 0.7\,\mathrm{nH}$, $C_\mathrm{min} = 0.47\,\mathrm{pF}$, $C_\mathrm{max} = 2.35\,\mathrm{pF}$ [11].

3 Numerical Results

The following parameters have been considered in the numerical evaluations if not otherwise specified: $f_0 = 2.4\,\mathrm{GHz}$, $R = 75\,\Omega$, $\mathbf{G}_\mathrm{R} = 0\,\mathrm{dB}$, $W = 80\,\mathrm{MHz}$. Half-wave dipoles with vertical polarization (z-axis) have been considered for the analytical evaluation of the impedance matrix

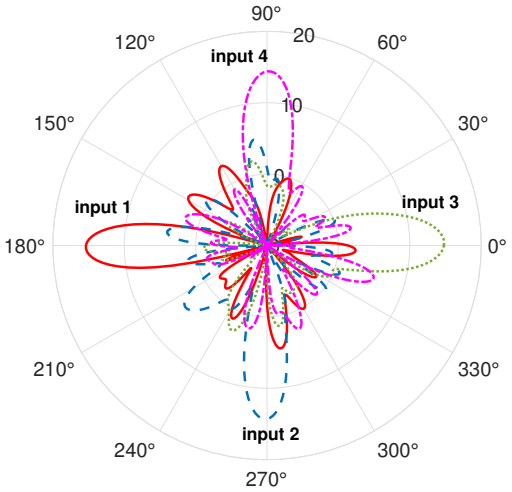

Figure 2. Single-carrier beam forming with $N_{\mathrm{A}} = 4$ RF chains.

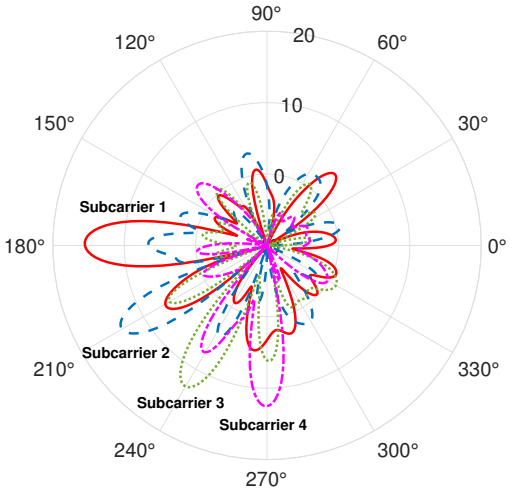

Figure 3. Multi-carrier beam forming with one RF chain ($N_{\mathrm{A}} = 1$) and $K = 4$ subcarriers.

$\mathbf{Z}^{(k)}$ at each subcarrier's frequency [10]. The scatterers of the DSA were deployed according to $L = 7$ concentric circles with an incremental radius of step $\Delta = \lambda_0/4$ and separated of $\lambda/4$ along the circle and the y axis corresponding to $N_{\mathrm{S}} = 214$ scatterers, where λ_0 denotes the wavelength at f_0. Numerical investigations have put evidence that the spacing $\Delta = \lambda_0/4$ results in a better performance [7]. This disk-like structure appears very appealing especially for its use in base stations or access points thanks to its circular symmetry. Obviously, other structures, even 3D, can be considered as well depending on the specific application.

We first investigate the single-carrier beam forming capabilities of the DSA using $N_{\mathrm{A}} = 4$ RF chains (inputs). A uniform set of $T = 108$ test points $\mathbf{p}_t = [d\sin\phi_t, 0, d\cos\phi_t]^{\mathrm{T}}$ on the $x-z$ plane a distance $d = 100\,\mathrm{m}$ (far-field region) was considered, with $\phi_t = 2\pi t/T$. The purpose is to associate a narrow beam radiation diagram to each RF chain (i.e., data stream) steering towards a specific angle, respectively, 180°, 270°, 0°, and 90°. This can be achieved by setting $[\mathbf{H}_{\mathrm{opt}}{}^{(1)}]_{(t_i,i)} = 1$, for $i = 1, 2, \ldots N_{\mathrm{A}}$ and zero otherwise, where t_i denotes the index of the test point corresponding to the ith steering angle. The standard numerical tool based on the quasi-Newton method with 5000 iterations has been utilized to minimize (3).

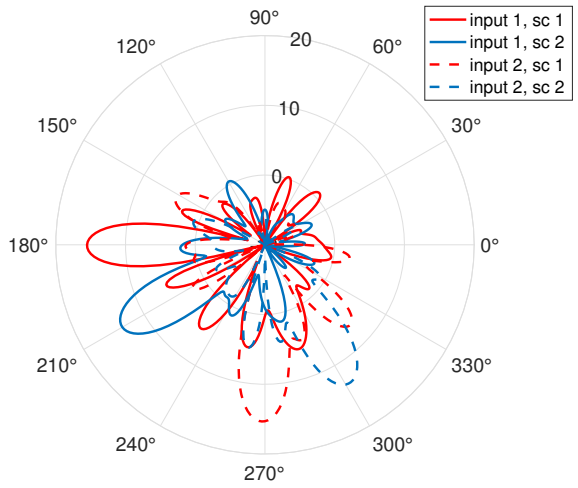

Figure 4. Joint angle-frequency beamforming $N_{\mathrm{A}} = 2$ RF chains and $K = 2$ subcarriers.

In Fig. 2, the radiation diagrams for the 4 steering angles are shown. As it can be observed, the gain of the DSA is independent of the angle and it is about $16-17\,\mathrm{dB}$. In addition, limited back radiation is obtained without the need to insert a ground plane that would impede the steering in the opposite direction. The DSA exhibits superdirectivity capability with an additional gain of about 5 dB with respect to a conventional array with the same aperture of the DSA. Contrary to standard arrays, where superdirectivity is obtained only in the end-fire direction [12], superdirectivity is notably obtained in all steering directions. Further examples of DSA design for single-carrier systems to realize superdirective beamforming, and MIMO precoding can be found in [7].

The capability of the DSA to provide frequency-selective radiation diagrams can be observed in Fig. 3, where $K = 4$ subcarriers where considered each of them associated with a different steering angle, respectively, 180°, 210°, 240°, and 270°, respectively. Compared to the single-carrier situation, the diagrams present slightly higher sidelobes indicating that managing wideband signals with the same configuration parameters of the DSA is more challenging.

Finally, the joint space-frequency performance of the DSA is reported in Fig. 4 obtained with $N_{\mathrm{A}} = 2$ RF chains and $K = 2$ subcarriers. The target steering angles for each input/subcarrier (sc) combination are: 180° (input 1, sc 1), 210° (input 1, sc 2), 270° (input 2, sc 1), and 300° (input 2, sc 2). The plots show that with the same configuration $\boldsymbol{\theta}$, obtained from the minimization of (3), the DSA is capable of associating a dedicated superdirective beam to each input/subcarrier combination.

Table 1

Fig. 2			
Configuration	Gain (dB)	η_1	η_2
input 1	17	0.82	0.68
input 2	16	0.84	0.68
input 3	16.3	0.88	0.71
input 4	16.3	0.82	0.64
Fig. 3			
Configuration	Gain (dB)	η_1	η_2
sc 1	16.7	0.97	0.83
sc 2	15.1	0.97	0.69
sc 3	15.3	0.98	0.56
sc 4	15.7	0.92	0.48
Fig. 4			
Configuration	Gain (dB)	η_1	η_2
input 1, sc 1	16.6	0.95	0.78
input 2, sc 2	15.9	0.95	0.60
input 2, sc 1	16.5	0.94	0.77
input 2, sc 2	15.6	0.97	0.59

The gain and efficiency of the DSA for the cases analyzed before, is reported in Table 1. In particular, η_1 and η_2 represent, respectively, the efficiency in case of a lossless DSA caused by imperfect impedance matching at the input ports and the overall efficiency accounting also for the losses. As can be noticed, most of the efficiency decreases due to the losses indicating that a discrete impedance matching is typically achieved during the optimization process.

4 Conclusion

In this paper, we have explored a frequency-selective dynamic scattering array (DSA) as a promising technology designed to shift signal processing tasks from the digital domain to the EM domain. This is achieved through the joint optimization of EM processing and the radiation of a few active and many reconfigurable scattering elements interacting within the reactive near field. The DSA offers an interesting capability to manage the EM field. This enables greater flexibility compared to traditional MIMO and recent SIM implementations. By minimizing the number of RF chains, DSA facilitates the development of energy-efficient, low-latency, and cost-effective holographic MIMO systems, addressing the sustainability challenges of future wireless networks.

Acknowledgment

This work was supported by the European Union under the Italian National Recovery and Resilience Plan (NRRP) of NextGeneration EU, partnership on “Telecommunications of the Future" (PE00000001 - program “RESTART"), and by the HORIZON-JU-SNS-2022-STREAM-B-01-03 6G-SHINE project (Grant Agreement No. 101095738).

References

[1] M. D. Renzo and M. D. Migliore, “Electromagnetic signal and information theory,” *IEEE BITS the Information Theory Magazine*, pp. 1–13, 2024.

[2] E. Björnson, C.-B. Chae, J. Heath, Robert W., T. L. Marzetta, A. Mezghani, L. Sanguinetti, F. Rusek, M. R. Castellanos, D. Jun, and Ö. Tugfe Demir, “Towards 6G MIMO: Massive Spatial Multiplexing, Dense Arrays, and Interplay Between Electromagnetics and Processing,” *arXiv e-prints*, p. arXiv:2401.02844, Jan. 2024.

[3] D. Dardari, G. Torcolacci, G. Pasolini, and N. Decarli, “An overview on over-the-air electromagnetic signal processing,” 2024. [Online]. Available: https://arxiv.org/abs/2412.14968

[4] D. Dardari, “Reconfigurable electromagnetic environments: A general framework,” *IEEE Journal on Selected Areas in Communications*, vol. 42, no. 6, pp. 1479–1493, June 2024.

[5] A. Silva, F. Monticone, G. Castaldi, V. Galdi, A. Alù, and N. Engheta, “Performing mathematical operations with metamaterials,” *Science*, vol. 343, no. 6167, pp. 160–163, 2014. [Online]. Available: https://science.sciencemag.org/content/343/6167/160

[6] J. An, C. Xu, D. W. K. Ng, G. C. Alexandropoulos, C. Huang, C. Yuen, and L. Hanzo, “Stacked intelligent metasurfaces for efficient holographic MIMO communications in 6G,” *IEEE Journal on Selected Areas in Communications*, vol. 41, no. 8, pp. 2380–2396, 2023.

[7] D. Dardari, “3D electromagnetic signal processing,” in *Proc. Asilomar Conf. on Signals, Systems and Computers*, Oct 2024.

[8] R. Harrington, “Reactively controlled directive arrays,” *IEEE Trans. Antennas Propag.*, vol. 26, no. 3, pp. 390–395, May 1978.

[9] J. C. Bucheli Garcia, M. Kamoun, and A. Sibille, “Low-complexity adaptive spatial processing of ESPAR antenna systems,” *IEEE Trans. Wireless Commun."*, vol. 19, no. 6, pp. 3700–3711, Feb. 2020.

[10] C. A. Balanis, *Antenna Theory: Analysis and Design*. New Jersey, USA: Wiley, 2016.

[11] S. Abeywickrama, R. Zhang, Q. Wu, and C. Yuen, “Intelligent reflecting surface: Practical phase shift model and beamforming optimization,” *IEEE Transactions on Communications*, vol. 68, no. 9, pp. 5849–5863, 2020.

[12] M. T. Ivrlac and J. A. Nossek, “The multiport communication theory,” *IEEE Circuits and Systems Magazine*, vol. 14, no. 3, pp. 27–44, 2014.